2012

Influence of Capillary Heterogeneity on Leakage of Co2 From a Borehols

Frank Roecker

INFLUENCE OF CAPILLARY HETEROGENEITY ON LEAKAGE OF CO2 FROM A BOREHOLE

A Thesis
presented in partial fulfillment of requirements
for the degree of Masters of Engineering Science
in the Department of Geology and Geological Engineering
The University of Mississippi

by

FRANK G. ROECKER

May 2012

ABSTRACT

We used a modified invasion percolation (MIP) model to examine the effect of capillary heterogeneity, buoyancy forces, and viscous forces on the surface area and saturation of a CO_2 plume leaking into a shallow aquifer. The purpose of this study is to provide a better understanding of how CO_2 migrates from a borehole, which is essential in implementing effective simulation and monitoring regimes to accurately detect CO_2 leakage from sequestration sites. The MIP model approach will simulate invasion of a light non-wetting fluid (e.g., CO_2) into a medium initially saturated with a dense wetting fluid (water). The style of capillary heterogeneity, the strength of buoyancy and viscous forces, and the size of the CO_2 source were systematically varied yielding 168 different simulation scenarios. We find that the interplay between capillary heterogeneity, buoyancy forces, and viscous forces controls the surface area and saturation of gaseous CO_2 leaking into an aquifer system. In unstructured systems with the absence of buoyancy and viscous forces, the CO_2 surface area and saturation are relatively large. In most cases, the CO_2 surface area decreases in weakly stratified systems, and as stratification increases, the CO_2 surface area increases and the CO_2 saturation decrease. Buoyancy forces stretch the invading CO_2 into a narrower structure, resulting in a higher surface area and a lower saturation. Our model implements weak viscous forces which cause CO_2 to pool around the leak source until, at a radial distance, either buoyancy or capillary forces begin to dominate CO_2 invasion. The dissolution rate of gaseous CO_2 into groundwater is proportional to the surface area of the CO_2 phase. Our study shows that variations in the style of capillary heterogeneity and

the strength of buoyancy and viscous forces can lead to large differences in CO_2 dissolution rates.

ACKNOWLEDGMENTS

This research was supported financially by the U.S. Department of Energy (U.S. DOE) and SSEB through the Southeast Regional Carbon Sequestration Partnership (SECARB) Phase III project.

I am grateful for my committee members Dr. Gregg Davidson and Dr. Joel Kuszmaul for their continued assistance and direction with this project. I would like to thank my graduate advisor, Dr. Robert Holt, for his guidance and support throughout this project.

Lastly, I would like to thank my family and friends for all of their encouragement over the years.

TABLE OF CONTENTS

LIST OF FIGURES

I. INTRODUCTION

Carbon capture and sequestration in deep geologic formations is emerging as a possible way to reduce greenhouse gas concentrations. Proposed sequestration sites are commonly located in depleted oil and gas fields, saline aquifers, or deep un-mineable coal seams (*Ide et al*., 2006; *Folger*, 2009, *Birkholzer et al*., 2009). On closure, most CO_2 sequestration sites will contain numerous well bores that penetrate cap-rocks of reservoirs and CO_2 sequestration horizons. Degradation of well-bore casing, plugs, and cements can create pathways for buoyant CO_2 to migrate towards the surface (*Ide et al*., 2006). The consequences of CO_2 leakage from a storage reservoir include the contamination of shallow potable water sources and the direct or delayed release of CO_2 gas back into the atmosphere, negating the long term effects of CO_2 sequestration.

Many researchers (e.g., *Ide et al*., 2006; *Bachu and Celia*, 2009; *Kopp et al*., 2010; *Tao et al*., 2011; *Zhang and Bachu*., 2011) have identified leakage along well bores as the most likely pathway for CO_2 leakage from a storage reservoir. These workers have developed models that explore CO_2 leakage from abandoned wells [*Kopp et al*., 2010; *Nordbotten et al*., 2005; *Humez et al*., 2011], along the annular cement [*Bachu and Bennion*, 2009; *Viswanathan et al*., 2008], and through multiple geological layers and multiple leaky wells [*Nordbotten et al*., 2009]. Others have focused on how the well-bore cement reacts in a CO_2 saturated environment [*Carey et al*., 2007; *Carey et al*., 2010; *Huerta et al*., 2011; *Geloni et al*., 2011]. Upon leakage from a well bore, escaped CO_2 may come into contact with shallow aquifers and migrate through the porous medium away from the well bore (e.g., *Oldenburg et al*., 2010). CO_2 dissolution into groundwater can lower pH, altering the aquifer geochemistry [*Wang and Jaffe*., 2004; *Zheng et al*., 2009; *Kharaka et al*., 2010; *Keating et. al*., 2010; *Peter et al*., 2011] and possibly triggering movement of trace metals [*Apps et al*., 2010; *Peter et al*., 2011].

Direct detection of CO_2 leakage in the shallow subsurface can be difficult due to large variations in natural background CO_2 fluxes (*Lewicki et al*., 2007). Other workers [*Romanak et al*, 2010; *Romanak et al*, 2012] have suggested that well-bore leaks into aquifers may be identified through long-term monitoring of groundwater. Measuring accurate amounts of dissolved CO_2 in groundwater is difficult, (*Newell et al*., 2008), but solute plumes containing newly dissolved minerals may be more readily identified (*Benson and Cole*, 2008). The character of solute plumes resulting from CO_2-driven alteration of aquifer materials will vary with the local CO_2 dissolution rate and the total mass of CO_2 within the aquifer, which control the evolution of aquifer pH near leaking boreholes. The dissolution rate of CO_2 into groundwater is limited by the surface area of the CO_2-groundwater interface, and the mass of CO_2 within the aquifer is a function of the CO_2-phase saturation. CO_2-phase saturation and surface area are directly influenced by the capillary heterogeneity within the aquifer, the magnitude of local buoyancy forces, and the influence of viscous forces arising from the displacement of groundwater by CO_2.

We examine the effect of capillary heterogeneity, buoyancy forces, and viscous forces on the surface area and saturation of a CO_2 plume in a shallow aquifer, resulting from a slow well-bore leak. The displacement of the denser wetting phase (e.g., water) by a lighter non-wetting phase (e.g., CO_2 gas) is simulated using a quasi-3D, Modified Invasion Percolation (MIP) model [e.g., *Ioannidis et al*., 1996; *Glass et al*., 2001; *Holt*, 2003] that includes capillary forces, buoyancy forces, and a first-order approximation of viscous forces. Over 8,400 simulations are employed in a Monte Carlo approach used to quantify the influence of and uncertainty due to variations in capillary heterogeneity, buoyancy forces, and viscous forces on CO_2 surface area and saturation. The style of capillary heterogeneity is systematically varied from unstructured to stratified to mimic the range of capillary heterogeneity found in nature. Similarly, the strength of buoyancy and viscous forces are also varied, and the influence of the leak source size is evaluated. All simulations are non-dimensional and can be scaled using the gas-entry pressure of a porous medium.

We find that the interplay between capillary heterogeneity, buoyancy forces, and viscous forces controls the surface area and saturation of gaseous CO_2 derived from well-bore leaks in aquifer systems. In stratified systems, the CO_2 surface area increases and the CO_2 saturation decreases with increasing stratification and buoyancy forces, both of which focuses CO_2 invasion into narrow pathways. CO_2 surface area decreases and CO_2 saturation increases in the presence of viscous forces, which leads to pooling of CO_2 near the source. As the leak source size increases, CO_2 invades along more pathways near the source, increasing the CO_2 surface area and saturation.

II. MODIFIED INVASION PERCOLATION MODEL

An MIP approach is used to simulate invasion of a light non-wetting fluid (gas) into a medium initially saturated with a dense wetting fluid (water) under the combined influence of capillary, buoyancy, and viscous forces. Compressibility and dissolution of CO_2 phase, trapping, and other dynamic effects, such as fragmentation and pulsation [e.g., *Wagner et al*., 1997; *Vedvik et al*., 1998; *Glass and Yarrington*, 2003], are neglected here, as our focus is on the broad factors affecting CO_2 dissolution rates and concentrations in aquifer systems. The current MIP differs from Invasion Percolation (IP) [e.g., *Wilkinson and Willemsen*, 1983] through the definition of macro, near-pore scale capillarity. Here, individual pore throats and necks are not considered. Instead, a near-pore scale block is defined and characterized by a local threshold spanning pressure (a local block-scale breakthrough pressure) that represents the behavior of the subscale network (*Holt et al*., 2003). The model domain is discretized into an array of grid blocks with assigned spanning pressures. The invasion pressure for each block is determined by the sum of the spanning pressure, gravity forces, and viscous forces:

$$P_I^* = P_S^* + \Delta\rho g Z^* + \Delta P_v^* \qquad (1)$$

where P_S^* is the capillary spanning pressure ($ML^{-1}T^{-1}$), $\Delta\rho = \rho_{defender} - \rho_{invader}$ is the difference in densities of the defending phase and invading phase (ML^{-3}), g is the acceleration due to gravity in the Z-direction (LT^{-2}), Z^* is the coordinate in the Z-direction (L), and $\Delta P_v^* = \left(P_v^{defender^*} - P_v^{invader^*}\right)$ is the difference in viscous pressure ($ML^{-1}T^{-1}$). Dividing equation (1) by the average spanning pressure $\langle P_S^* \rangle$, our dimensionless invasion pressure becomes:

$$P_I = \frac{P_S^*}{\langle P_S^* \rangle} + B_O Z + \frac{\left(P_v^{d*} - P_v^{i*}\right)}{\langle P_S^* \rangle} \tag{2}$$

where $\langle P_S^* \rangle$ is the average spanning pressure ($ML^{-1}T^{-1}$), the dimensionless Bond Number is defined as:

$$B_O = \frac{\Delta \rho g \Delta Z^*}{\langle P_S^* \rangle} \tag{3}$$

ΔZ^* is the grid block length in the Z-direction (L). The dimensionless Z-coordinate is defined as:

$$Z = \frac{Z^*}{\Delta Z^*} \tag{4}$$

The Bond Number reflects the strength of the buoyancy forces. For the simulations presented here, the Bond Number was systematically varied between 0, 0.1, and 1 to represent increasing buoyancy forces.

The viscous pressure in the defending fluid was set at zero for all simulations, to simulate static, non-flowing groundwater conditions. The viscous pressure in the invading fluid is calculated by a first-order approximation for steady flow from a point source in spherical coordinates with the reduced equation being:

$$\frac{P_v^{i*}}{\langle P_S^* \rangle} = VSN\left(\frac{1}{r} - \frac{1}{R}\right) \tag{5}$$

where *VSN* is the dimensionless viscous scaling number, *r* is the dimensionless grid-block radial coordinate (-), and *R* is the dimensionless radius of influence (-). An *R* value of 1000 was kept constant for all simulations. We selected *VSN* values of 0 and 250; a *VSN* value of 250 is equivalent to a CO_2 volumetric discharge rate of 0.03 m^3/d in a typical sandstone and 3×10^{-4} m^3/d in a typical mudrock or shale.

Correlated spanning-pressure fields are generated using an FFT approach (e.g., Robin et al., 1993). First, a two-dimensional, correlated random field (512 by 512) with a standard-normal distribution is generated, then the value at each nodal location is mapped to an associated probability, and finally the nodal spanning pressure is determined from the nodal probability (P) using the van Genuchten (1980) pressure-saturation model:

$$P_S = \frac{1}{\alpha}\left\{\left[\left(\frac{1}{P}\right)^{\frac{1}{\frac{1}{1-\frac{1}{N}}}}\right] - 1\right\}^{\frac{1}{N}} \tag{8}$$

where P_s is the spanning pressure, α is a model parameter related to the air-entry pressure, N is a model parameter associated with the pore-size distribution. Alpha (α) values of 1 and N values of 1.5 were kept constant for all simulations. The style of capillary heterogeneity in each field is defined by a fixed correlation ratio, the ratio of the horizontal to vertical correlation lengths. Correlation ratios of 1, 10, 20, 30, 50, 100, 500, and 1000 were used to reflect increasing horizontal stratification. Values of 1, 10, and 50 are used as the dimensionless vertical correlation lengths (Figure 1). As the vertical correlation length increases, the horizontal correlation lengths are increased to maintain specified correlation ratios.

During simulations, non-wetting phase invasion proceeds from a source on the left edge of the domain towards the top or right edge domain boundary according to an IP algorithm that implements equation (2). We apply a network connectivity of 8 (communication is allowed with all surrounding blocks) to approximate three-dimensional behavior within a two-dimensional network (e.g., Holt et al., 2003). The IP algorithm sorts all the invadable nodes along the wetted surface and invades the block with the lowest invasion pressure. This process continues until the blocks along the active interface reach either the top or right edge boundaries, the percolation threshold. In the absence of buoyancy and viscous forces ($B_O = 0$ and $\Delta P_v^* = 0$), standard percolation will exactly reproduce the drainage pressure-saturation curve given by equation (8) (*Holt et al*., 2003). However, when $\Delta P_v^* \neq 0$ and $B_O \neq 0$, this is not the case.

Our model simulates leakage from a point source and a line source along the left edge of the domain. The model defines an initial wetted surface of CO_2 that acts as the leak source. The wetted surface is defined as all the possible nodes that are in contact with the growing cluster. The initial wetted surface for a point source allows invasion of CO_2 only into the bottom-most node on the left-hand side of the domain. This small source size is analogous to CO_2 escaping through a fracture in the well-bore casing or cement. For the larger leak source, the bottom 102 nodes (10% of the domain size) along the left-hand side of the domain are considered invadable at the start of the simulation. This arrangement simulates CO_2 leaking from a well bore through degraded annular cement. Studies have shown that well-bore cement can degrade after 200 years to allow potential fluid flow analogues to that through a silty sand (*EPA*, 2009).

Simulations including viscous forces were only conducted for a point source in random spanning pressure fields with a vertical correlation length of 1 grid block, as more complicated source sizes and styles of heterogeneity would lead to greater errors in our first-order approximation.

In the following discussion, the term “surface area” is defined as the surface area per unit volume of invaded.

III. RESULTS

We focus on the final CO_2 surface area (ratio of the CO_2-water surface area to CO_2 volume) and the final CO_2 saturation at percolation to either the right or top boundary. 8,400 simulations were run to evaluate the influence of capillary heterogeneity, buoyancy forces, and viscous forces on the CO_2 surface area and saturation. 168 different combinations were created by varying the correlation ratio, Bond Number, strength of first-order viscous forces, the Z-correlation length, and leak source size (Table 1). 50 simulations were run for each combination. CO_2 surface area and saturation results are summarized using the average and standard deviation for each 50-simulation set.

Figures 2 and 3 show the influence of varying styles of stratification on the evolution of the CO_2 phase in the absence of buoyancy and viscous forces for the case of a point source and a line source, respectively. Both source sizes show similar results. For unstructured media (Z-correlation length of 1 and correlation ratio of 1), the CO_2 surface area is fairly large (~1) as the CO_2 phase distribution is controlled by the random distribution of spanning pressures. The addition of structure, in the form of either vertical or horizontal correlation, decreases the surface area (~0.6), as invasion fills adjacent grid blocks, which have similar spanning pressures. As the degree of stratification increases, the CO_2 surface area increases, reflecting less vertical overlap in the CO_2 phase. As the correlation ratio becomes large, invasion tends to proceed similarly regardless of the vertical correlation length, and the average surface areas for all vertical correlation lengths become similar. The average surface area from a line source (Figure 3) (~1.5) is greater than that of a point source (Figure 2) (~1.2) at large correlation ratios, as the i nvading CO_2 takes multiple pathways from the source. Average CO_2 saturation increases with increasing Z-correlation length, as regions of similar spanning pressure become completely filled with the invading CO_2. The average CO_2 saturation decreases with increasing correlation ratio, because CO_2 invasion becomes focused to fewer strata and the percolation threshold is reached in fewer invasion steps.

Figures 4 and 5 display how intermediate buoyancy forces ($B_O = 0.1$) affect CO_2 phase invasion from a point and a line force respectively. Both source sizes show similar results. For unstructured media (Z-correlation lengths of 1 and a correlation ratio of 1), the CO_2 surface area is fairly large (~1.3) and CO_2 saturation is low (~0.02), as the CO_2 phase is being stretched vertically into a narrow structure by buoyancy forces. When the vertical correlation ratio increases from 1 to 10 in un-stratified media, CO_2 fills adjacent grid blocks with similar spanning pressures, decreasing CO_2 surface area (~0.6) and slightly increasing CO_2 saturation (~0.03). When the vertical correlation length reaches 50, however, stronger vertical correlation of spanning pressures allows buoyancy forces to dominate the local capillary heterogeneity, leading to slightly higher surface areas.

For both leak source sizes (Figures 4 and 5), buoyancy forces become less influential over the CO_2 plume as the medium becomes more stratified, and the percolation threshold is reached on the right boundary. Instead of a narrow, vertical structure, the final CO_2 phase distribution reflects trapping beneath horizontal capillary barriers of higher spanning pressure. When the vertical correlation length is 1, buoyancy forces are strongest, leading to vertical stacking of CO_2-invaded layers, lower CO_2 surface areas, and higher CO_2 saturations. Weakly stratified systems (correlation ratio of 10) show lower surface areas (~0.7) and higher saturations (~0.05) than the unstructured systems, as CO_2 fills more vertically adjacent gridblocks. As stratification increases, CO_2 invasion proceeds along an increasingly horizontal pathway, increasing CO_2 surface area and decreasing CO_2 saturation. At large correlation ratios, the average surface area from a line source (Figure 5) (~1.5) is greater than that from a point source (Figure 4) (~1.2), because CO_2 can take multiple pathways from the source.

Figures 6 and 7 show how strong buoyancy forces (B_O = 1) affect CO_2 invasion from a point source and from a line source, respectively. Both source sizes show similar results. In unstructured media (Z-correlation lengths of 1 and a correlation ratio of 1), the CO_2 surface area is very large (~2.2) and the CO_2 saturation is very low (~0.004), because the CO_2 phase is being stretched vertically into a very narrow structure. In weakly stratified systems, buoyancy forces remain strong relative to capillary forces, and vertical stacking of CO_2-invaded layers causes lower surface areas (~0.8 for Z = 1) and slightly higher saturations (~0.025 for Z = 1). This process is particularly important for simulations run with a vertical correlation length of 1, where strong buoyancy forces lead to percolation at the upper boundary and increased vertical stacking to correlation ratios of 30 and 50. As the correlation ratios increase, horizontal capillary forces dominate the system, vertical stacking is reduced, and the percolation threshold is quickly reached at the right boundary; under these conditions, CO_2 surface areas increase, and CO_2 saturations decrease. The CO_2 surface areas for line sources are generally slightly larger than those observed from point sources.

The influence of viscous forces on CO_2 invasion with increasing levels of stratification and increasing buoyancy forces from a point source is show in Figures 8. Here, results for VSN = 250 and a vertical correlation length of 1 are presented. Viscous forces lead to pooling of CO_2 around the source, which decreases CO_2 surface area and increases CO_2 saturation when compared with the results for simulations where viscous forces are absent (e.g., Figures 2, 3, and

6). The effect of CO_2 pooling is most apparent in strongly stratified systems, where the CO_2 surface area is greatly reduced (~0.7) when compared with simulations without viscous forces. For example, in Figure 2, where CO_2 invasion is only controlled by spanning pressures, CO_2 surface areas were around 1.2 in strongly stratified systems (correlation ratio of 1000). As buoyancy forces were increased, the CO_2 surface area increases to ~1.2 and ~1.5 at Bond Numbers of 0.1 (Figure 4) and 1 (Figure 6), respectively.

The overall trends observed in the surface area and saturation plots in Figure 8 are similar to those reported above. Here, the average CO_2 surface area in unstructured media increases as buoyancy forces are increased, while the average CO_2 saturation decreases. Increasing stratification initially leads to vertical stacking of CO_2 saturated layers, reducing the surface area. As stratification is increased further, the CO_2 surface area increases slightly, but does not reach the high values observed in the absence of viscous forces. When buoyancy forces are absent, CO_2 saturation is very large (~0.2), and then decreases as stratification increases. In the presence of buoyancy forces, saturations peak (~0.08) in weakly stratified media as CO_2 is vertically stacked in overlapping layers. As stratification increases, CO_2 invasion becomes more strongly focused into horizontal layers, reducing saturations (~0.02).

The coefficient of variation (C_v) of the CO_2 surface area (Figure 9) reflects the relative uncertainty in the average CO_2 surface area. The pattern of the surface area C_v versus correlation ratio or stratification strength is varies mainly with the vertical correlation length. When the vertical correlation length is 1 (Figure 9a), the C_v generally increases as stratification becomes stronger. Here, the unstructured systems are more closely ergodic, and the systems become less ergodic (more variability in invasion pathways) as the correlation ratio increases. When the vertical correlation length is 10 (Figure 9b), the surface area C_v initially increases and then decreases, as stratification becomes stronger, reflecting a shift from mainly upward to dominantly horizontal invasion patterns. When the vertical correlation length is 50 (Figure 9c), the surface area C_v generally decreases with increasing stratification, as CO_2 invasion proceeds along increasingly narrow, horizontal pathways. The surface area C_v during CO_2 invasion with viscous forces into media with a vertical correlation length of 1 is similar to that observed in Figure 9a, indicating that the addition of viscous forces does not lead to significantly different CO_2 invasion patterns between simulations.

In general, the uncertainty increases when B_o increases from 0 to 0.1, as CO_2 invasion pathways are pulled upward by buoyancy forces. A further increase in B_o from 0.1 to 1, generally leads to a decrease in the uncertainty, as invasion is focused into narrower pathways.

Our results show that the interplay between capillary heterogeneity, buoyancy forces, and viscous force controls the dissolution rate and aqueous concentrations of CO_2 derived from well-bore leaks in aquifer systems. The dissolution rate of gaseous CO_2 into groundwater is proportional to the surface area of the CO_2 phase. Our study shows that variations in the style of capillary heterogeneity and the strength of buoyancy and viscous forces can lead to differences in CO_2 dissolution rates of well over an order of magnitude (factor of ~17 in this study). Depending on the scenario, the CO_2 surface area increases by a factor between 3 and 9, as the degree of stratification increases. As buoyancy forces increase (from B_o = 0 to B_o = 1), the CO_2 surface area typically increases by a factor of ~2. The addition of weak viscous forces lowers the CO_2 surface area by a factor of 1.1 in unstructured media and a factor of 2 in well stratified media. Changing from a point to a line source can increase CO_2 surface areas by a factor of 1.3.

The CO_2 saturation is a metric for the dissolved CO_2 concentration in groundwater, assuming all gaseous CO_2 is dissolved into groundwater, and the geochemical impact of the CO_2

well-bore leak, as high CO_2 saturations will eventually lead to high dissolved CO_2 concentrations. Increasing stratification decreases CO_2 saturation by a factor of between 8 and 60, depending upon the scenario. The addition of strong buoyancy forces (B_o = 1) decreases CO_2 saturation by a factor of 23 to 35 in unstructured media. Strong buoyancy forces reduce saturations by a factor of 1.2 to 3.6 in weakly-stratified media, and increase saturations by a factor of 1.1 to 2.5 in well-stratified media. Saturations increase by factors between 1.2 and 6, when weak viscous forces are added. The presence of a line source, rather than a point source, can increase CO_2 saturations by up to a factor of 4.

IV. SUMMARY AND DISCUSSION

We used a quasi-3D, MIP model to examine the effect of capillary heterogeneity, buoyancy forces, and first-order viscous forces on the surface area (per unit volume) and saturation of a CO_2 plume in a shallow aquifer, resulting from a slow well-bore leak. Compressibility and dissolution of CO_2 phase, trapping, and other dynamic effects, such as fragmentation and pulsation, were neglected. The style of capillary heterogeneity, the strength of buoyancy and viscous forces, and the size of the CO_2 source were systematically varied yielding 168 different scenarios. Each scenario was then simulated 50 times and the CO_2 surface area and saturation was determined. The style of capillary heterogeneity was systematically varied from unstructured to stratified to mimic the range of capillary heterogeneity found in nature.

We find that the CO_2 surface area and saturation is governed by the interplay between capillary heterogeneity, buoyancy forces, and viscous forces. In stratified systems, the CO_2 surface area increases and the CO_2 saturation decreases with increasing stratification and buoyancy forces, both of which focuses CO_2 invasion into narrow pathways. Viscous forces, which lead to pooling of the CO_2 near the source, lead to lower CO_2 surface area and higher CO_2 saturation. As the leak source size increases, CO_2 invades along more pathways near the source, increasing the CO_2 surface area and saturation. Variations in the style of capillary heterogeneity and the strength of buoyancy and viscous forces can lead to differences in CO_2 dissolution rates of well over an order of magnitude, and CO_2 saturations can vary by nearly two orders of magnitude.

Our results provide critical insight into the processes affecting CO_2 dissolution rates and aqueous CO_2 concentrations resulting from well-bore leaks into groundwater aquifers and can inform continuum-based modeling of well-bore leak processes and geochemical reactions within the aquifer. Knowledge of the style of capillary heterogeneity and the strength of buoyancy and viscous forces is essential for determining apparent diffusion coefficients and dissolution rates for CO_2 gas into groundwater. The capillary pressure-saturation relationships used in most continuum-based models should be modified to include the impact of stratification, the directionality of the invasion process, and the strength of local buoyancy and viscous forces. Prior to modeling CO_2 dissolution processes in aquifer materials, site-specific geologic data (core descriptions, samples, etc.) are required to identify and characterize the extent of capillary heterogeneity.

Slow leaks from boreholes may be difficult to detect in well-stratified geologic materials, as high CO_2 dissolution rates and low CO_2 saturations may make geochemical changes in the aquifer difficult to identify. In unstructured (e.g., sedimentary media affected by bioturbation or pedogenesis) and weakly stratified materials, CO_2 well-bore leaks may be more readily identifiable from geochemical changes in groundwater, as CO_2 saturations will be higher.

LIST OF REFERENCES

V. REFERENCES

Apps, J. A., Zheng, L., Zhang, Y., Xu, T., Birkholzer, J. T. (2010), Evaluation of Potential Changes in Groundwater Quality in Response to CO_2 Leakage from Deep Geologic Storage, *Transp. Porous Med.*, *82*, 215-246.

Bachu, S. and Bennion, D. B. (2009), Experimental assessment of brine and/or CO_2 leakage through well cements at reservoir conditions, *Int. J. of Greenhouse Gas Control*, *3*, 494-501.

Bachu, S., and Celia, M. A. (2009), Assessing the Potential for CO_2 Leakage, Particularly Through Wells, From Geological Storage Sites, *Geophysical monograph*, 183, 203-216.

Benson, S. M., and Cole, D. R. (2008), CO_2 Sequestration in Deep Sedimentary Formations, *Elements*, *4*, 325-331.

Birkholzer, J. T., Zhou, Q., Tsang, C.F. (2009), Large-scale impact of CO_2 storage in deep saline aquifers: A sensitivity study on pressure response in stratified systems, *J. Greenhouse Gas Control*, *3*, 181-194.

Carey, J. W., Wigand, M., Chipera, S. J., WoldeGabriel, G., Pawar, R., Lichtner, P. C., Wehner, S. C., Raines, M. A., Guthrie Jr, G. D. (2007), Analysis and performance of oil well cement with 30 years of CO_2 exposure from the SACROC Unit, West Texas, USA, *Int. J. of Greenhouse Gas Control*, *1*, 75-85.

Carey, J. W., Svec, R., Grigg, R., Zhang, J., Crow, W. (2010), Experimental investigation of wellbore integrity and CO_2-brine flow along the casing-cement microannulus, *Int. J. of Greenhouse Gas Control*, *4*, 272-282.

U.S. Environmental Protection Agency (EPA). (2009), Title 40 CFR Part 191 Subparts B and C: Compliance Recertification Application for the Waste Isolation Pilot Plant Consideration of Drilling Events in Performance Assessment, pp. 33-1 through 33-23.

Folger, P. (2009). Carbon Capture and Sequestration (CCS), Congressional Research Service 7-5700.

Geloni, C., Giorgis, T., Battistelli, A. (2011), Modeling of Rocks and Cement Alteration due to CO_2 Injection in an Exploited Gas Reservoir, *Transp. Porous Med.*, *90*, 183-200.

Glass, R. J., Rajaram, H., Nicholl, M. J., Detwiler, R. L. (2001), The interaction of two fluid phases in fractured media, *Current Opinion in Colloid & Interface Science*, *6*, 223-235.

Glass, R. J., and Yarrington, L. (2003), Mechanistic modeling of fingering, nonmonotonicity, fragmentation, and pulsation within gravity/buoyant destabilized two-phase/unsaturated flow, *Water Resour. Res.*, *39*(3), 1058, doi:10.1029/2002WR1542.

Holt, R. M., Glass, R. J., Sigda, J. M., Mattson, E. D. (2003), Influence of centrifugal forces on phase structure in partially saturated media, *Geophys. Res. Lett.*, *30*(13), 1692, doi:10.1029/2003GL017340.

Huerta, N. J., Bryant, S. L., Strazisar, B. R., Hesse, M. (2011), Dynamic alteration along a fractured cement/cement interface: Implications for long term leakage risk along a well with an annulus defect, *Energy Procedia*, *4*, 5398-5405.

Humez, P., Audigane, P., Lions, J., Chiaberge, C., Bellenfant, G. (2011), Modeling of CO_2 Leakage up Through an Abandoned Well from Deep Saline Aquifer to Shallow Fresh Groundwaters, *Transp. Porous Med.*, *90*, 153-181.

Ide S. T., Friedmann, S. J., Herzog, H. J. (2006), CO_2 leakage through existing wells: current technology and regulations. Presented at the 8th International Conference on Greenhouse Gas Control Technologies, Trondeim, Norway, June.

Ioannidis, M. A., Chatzis, I., Dullien, F. A. L. (1996), Macroscopic percolation model of immiscible displacement: Effects of buoyancy and spatial structure, *Water Resour. Res.*, *32*(11), 3297-3310.

Keating, E. H., Fessenden, J., Kanjorski, N., Koning, D. J., Pawar, R. (2010), The impact of CO_2 on shallow groundwater chemistry: observations at a natural analog site and implications for carbon sequestration, *Environ. Earth Sci.*, *60*, 521-536.

Kharaka, Y. K., Thordsen, J. J., Kakouros, E., Ambats, G., Herkelrath, W. N., Beers, S. R., Birkholzer, J. T., Apps, J. A., Spycher, N. F., Zheng, L., Trautz, R. C., Rauch, H. W., Gullickson, K. S. (2010), Changes in the chemistry of shallow groundwater related to the 2008 injection of CO_2 at the ZERT field site, Bozeman, Montana, *Environ. Earth Sci.*, *60*, 273-284.

Kopp, A., Binning, P.J., Johannsen, K., Helmig, R., Class, H. (2010), A contribution to risk analysis for leakage through abandoned wells in geological CO_2 storage, *Adv. In Water Resour.*, *33*, 867-879.

Lewicki, J. L., Oldenburg, C. M., Dobeck, L., Spangler, L. (2007), Surface CO_2 leakage during two shallow subsurface CO_2 releases, *Geophys. Res. Lett.*, *34*, L24402, doi:10.1029/2007GL032047.

Newell, D. L., Kaszuba, J. P., Viswanathan, H. S., Pawar, R. J., Carpenter, T. (2008), Significance of carbonate buffers in natural waters reacting with supercritical CO_2: Implications for monitoring, measuring and verification (MMV) of geologic carbon sequestration, *Geophys. Res. Lett.*, *35*, L23403, doi:10.1029/2008GL035615.

Nordotten, J. M., Celia, M. A., Bachu, S., Dahle, H. K. (2005), Semianalytical Solution for CO_2 Leakage through an Abandoned Well, *Environ. Sci. Technol.*, *39*, 602-611.

Nordbotten, J. M., Kavetski, D., Celia, M. A., Bachu, S. (2009), Model for CO_2 Leakage Including Multiple Geological Layers and Multiple Leaky Wells, *Environ. Sci. Technol.*, *43*, 743-749.

Oldenburg, C. M., Lewicki, J. L., Dobeck, L., Spangler, L. (2010), Modeling Gas Transport in the Shallow Subsurface During the ZERT CO_2 Release Test, *Transp. Porous Med.*, *82*, 77-92.

Peter, A., Hornbruch, G., Dahmke, A. (2011), CO_2 leakage test in a shallow aquifer for investigating the geochemical impact of CO_2 on groundwater and for developing monitoring methods and concepts, *Energy Procedia*, *4*, 4148-4153.

Romanak, K. D., Smyth, R. C., Yang., C., Havorka, S. D., Lu., J. (2010), Role of dedolomitization in the detection of anthropogenic CO_2 in freshwater aquifers, paper presented at the Water Rock Interation 13 Conference, Guanajuatl, Mexico, Digital Publication Series #10-02, pp. 1-4.

Romanak, K. D., Smyth, R. C., Yang, C., Havorka, S. D., Rearick, M., Lu., J. (2012), Sensitivity of groundwater systems to CO_2: Application of a site-specific analysis of carbonate monitoring parameters at the SACROC CO_2-enhanced oil field, *Int. J. of Greenhouse Gas Control*, *6*, 142-152.

Tao, Q., Checkai, D., Huerta, N., Bryant, S. L. (2011), An Improved Model to Forecast CO_2 Leakage Rates Along a Wellbore, *Energy Procedi,, 4*, 5385-5391.

van Genuchten, M. T. (1980), A Closed-form Equation for Predicting the Hydraulic Conductivity of Unsaturated Soils, *Soil Sci. Soc. Am. J.*, *44*, 892-898.

Vedvik, A., Wagner, G., Oxaal, U., Feder, J., Meakin, P., Jøssang, T. (1998), Fragmentation Transition for Invasion Percolation in Hydraulic Gradients, *Phys. Rev. Lett.*, *80*, 3065-3068.

Viswanathan, H. S., Pawar, R. J., Stauffer, P. H., Kaszuba, J. P., Carey, J. W., Olsen, S. C., Keating, G. N., Kavetski, D., Guthrie, G. D. (2008), Development of a Hybrid Process and System Model for the Assessment of Wellbore Leakage at a Geologic CO_2 Sequestration Site, *Environ. Sci. Technol.*, *42*, 7280-7286.

Wagner, G., Meakin, P., Feder, J., Jøssang, T. (1997), Buoyancy-driven invasion percolation with migration and fragmentation, *Physica A*, *245*, 217-230.

Wang, S., and Jaffe, P. R. (2004), Dissolution of a mineral phase in potable aquifers due to CO_2 releases from deep formations; effect of dissolution kinetics, *Energy Convers. Manage.*, *45*, 2833-2848.

Wilkinson, D., and Willemsen, J. F. (1983), Invasion percolation: a new form of percolation theory, *J. Phys. A: Math. Gen.*, *16*, 3365-3376.

Zhang, M., and Bachu, S. (2011), Review of integrity of existing wells in relation to CO_2 geological storage: What do we know?, *Int. J. of Greenhouse Gas Control*, *5*, 826-840.

Zheng, L., Apps, J. A., Zhang, Y., Xu, T., Birkholzer, J. T. (2009), Reactive Transport Simulations to Study Groundwater Quality Changes in Response to CO_2 Leakage from Deep Geological Storage, *Energy Procedia*, *1*, 1887-1894.

List of Appendices

Appendix: A

Table 1.
Simulation variables and values

Viscous Scaling Number (VSN)	250
Leak Source Sizes	1, 102
Vertical Correlation Lengths	1, 10, 50
Correlation Ratios	1, 10, 20, 30, 50, 100, 500, 1000
Bond Number	0, 0.1, 1

Table 2. Summary of simulation results as changes to the CO_2 surface area and saturation. Values are factors of increase or decrease.

Increase	Surface Area	Saturation
Stratification	↑ 1.5	↓ 8-60
Vertical Correlation Length	↓ 3 – 4	↑ 1.3 – 1.6
Source Size	↑ 1.2 – 1.7	↑ 1.2 – 4
Buoyancy Forces	↑ 1.3 – 3.7	↓ 6.5 – 35
Viscous Forces	↓ 1.1 – 1.7	↑ 1.7 – 6.2

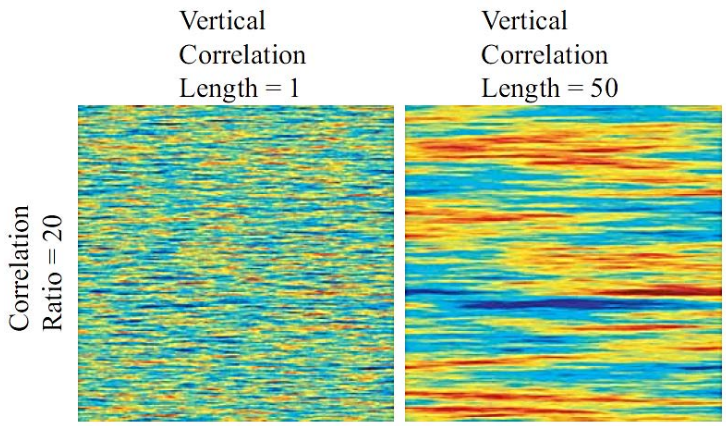

Figure 1. Random fields with (a) a horizontal correlation length of 20 and a vertical correlation length of 1, and (b) a horizontal correlation length of 100 and a vertical correlation length of 50. The horizontal correlation length will vary to maintain correlation ratios.

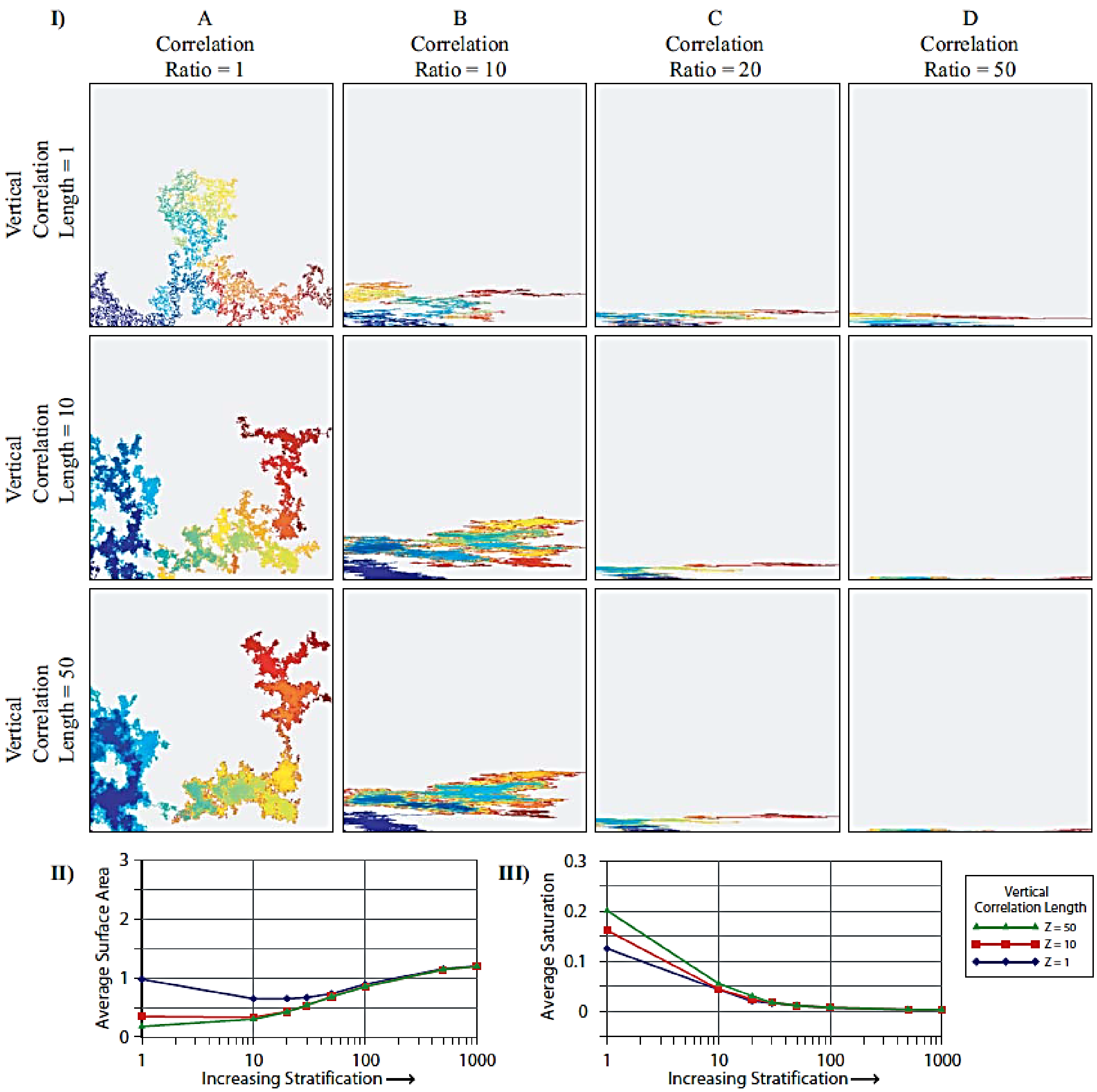

Figure 2. CO_2 invasion history (I) from a point source in the absence of buoyancy forces and viscous forces in (a) unstructured media, (b) weakly stratified media, (c) more stratified media, and (d) highly stratified media. Invasion pictures for correlation ratios of 100, 500, and 1000 are not shown because the invasion phase only populates a few layers near the bottom of the domain. CO_2 invasion progress from early to late is reflected by the progression of dark to light colors. Grid blocks saturated with the wetted phase are shown in gray. Plots displaying the (II) average surface area, and (III) average saturation for theses simulations versus increasing stratification. The average saturation is plotted between -0.5 to 0.3 to clearly illustrate results close to zero. No simulations produced saturations less than zero.

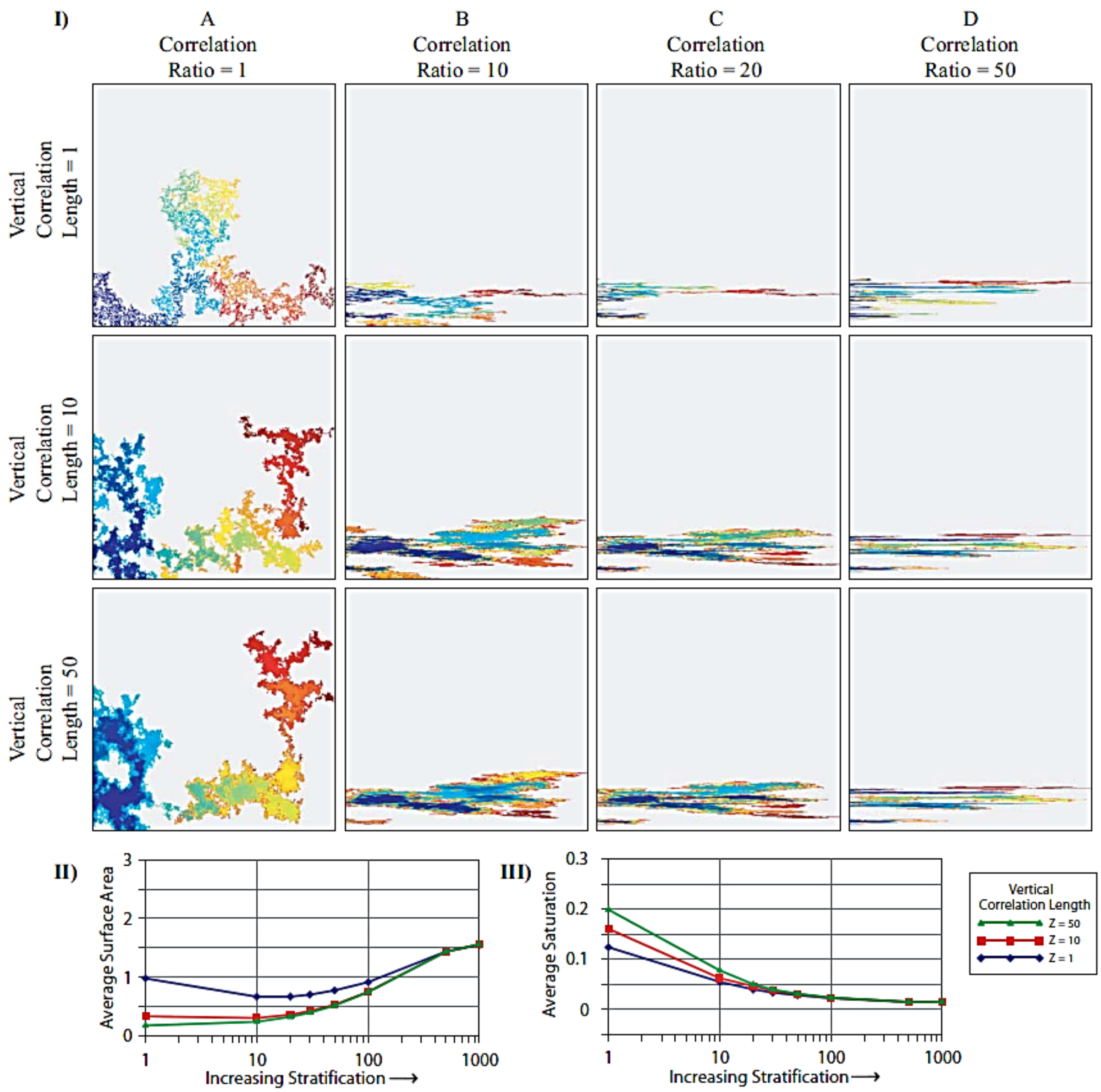

Figure 3. CO_2 invasion history (I) from a line source with a Bond Number = 0 in (a) unstructured media, (b) weakly stratified media, (c) more stratified media, and (d) highly stratified media. Invasion pictures for correlation ratios of 100, 500, and 1000 are not shown because the invasion phase only populates a few layers near the bottom of the domain. CO_2 invasion progress from early to late is reflected by the progression of dark to light colors. Grid blocks saturated with the wetted phase are shown in gray. Plots displaying the (II) average surface area, and (III) average saturation for theses simulations versus increasing stratification. The average saturation is plotted between -0.5 to 0.3 to clearly illustrate results close to zero. No simulations produced saturations less than zero.

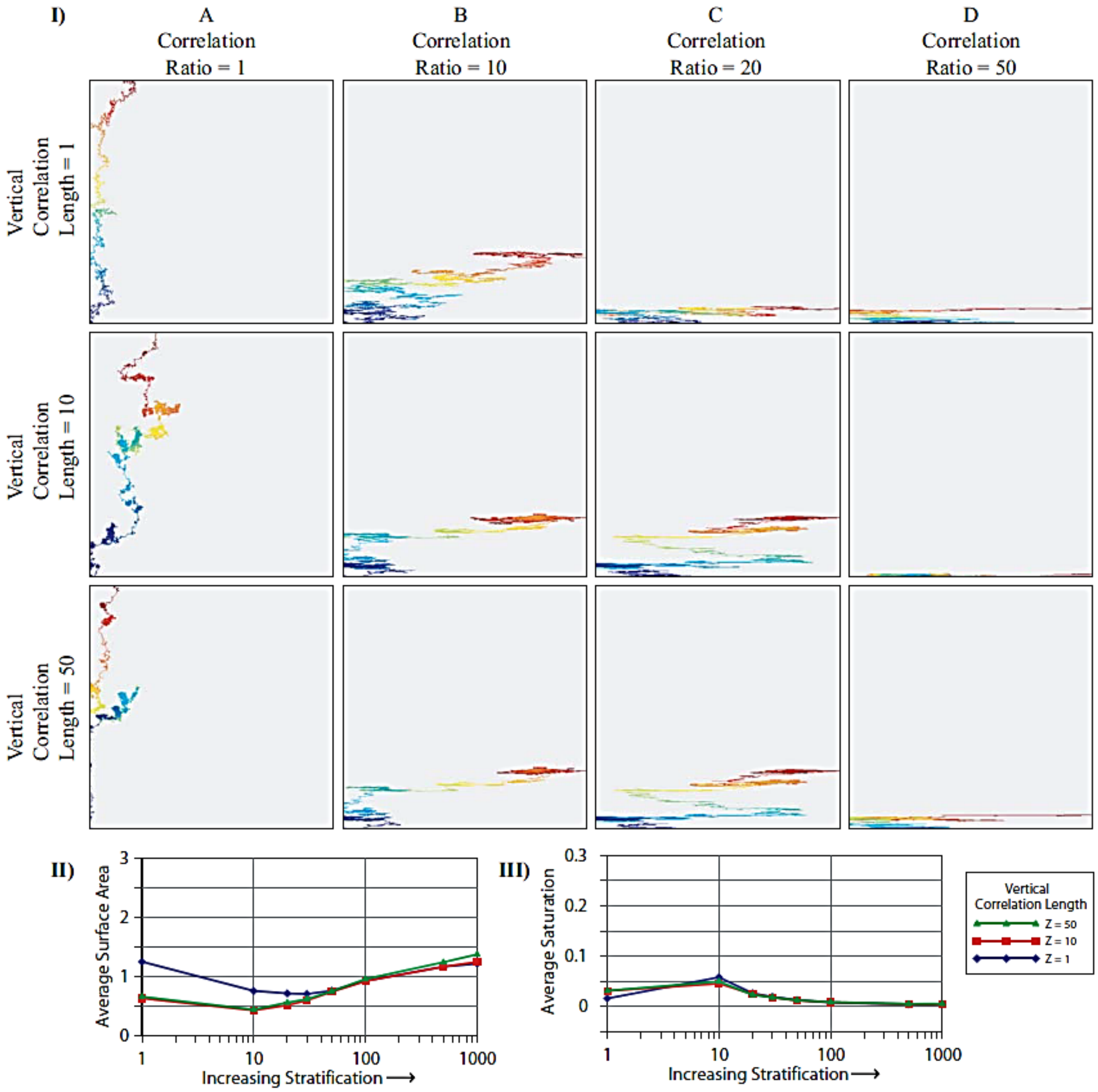

Figure 4. CO_2 invasion history (I) from a point source with a Bond Number = 0.1 and no viscous forces in (a) unstructured media, (b) weakly stratified media, (c) more stratified media, and (d) highly stratified media. Invasion pictures for correlation ratios of 100, 500, and 1000 are not shown because the invasion phase only populates a few layers near the bottom of the domain. CO_2 invasion progress from early to late is reflected by the progression of dark to light colors. Grid blocks saturated with the wetted phase are shown in gray. Plots displaying the (II) average surface area, and (III) average saturation for theses simulations versus increasing stratification. The average saturation is plotted between -0.5 to 0.3 to clearly illustrate results close to zero. No simulations produced saturations less than zero.

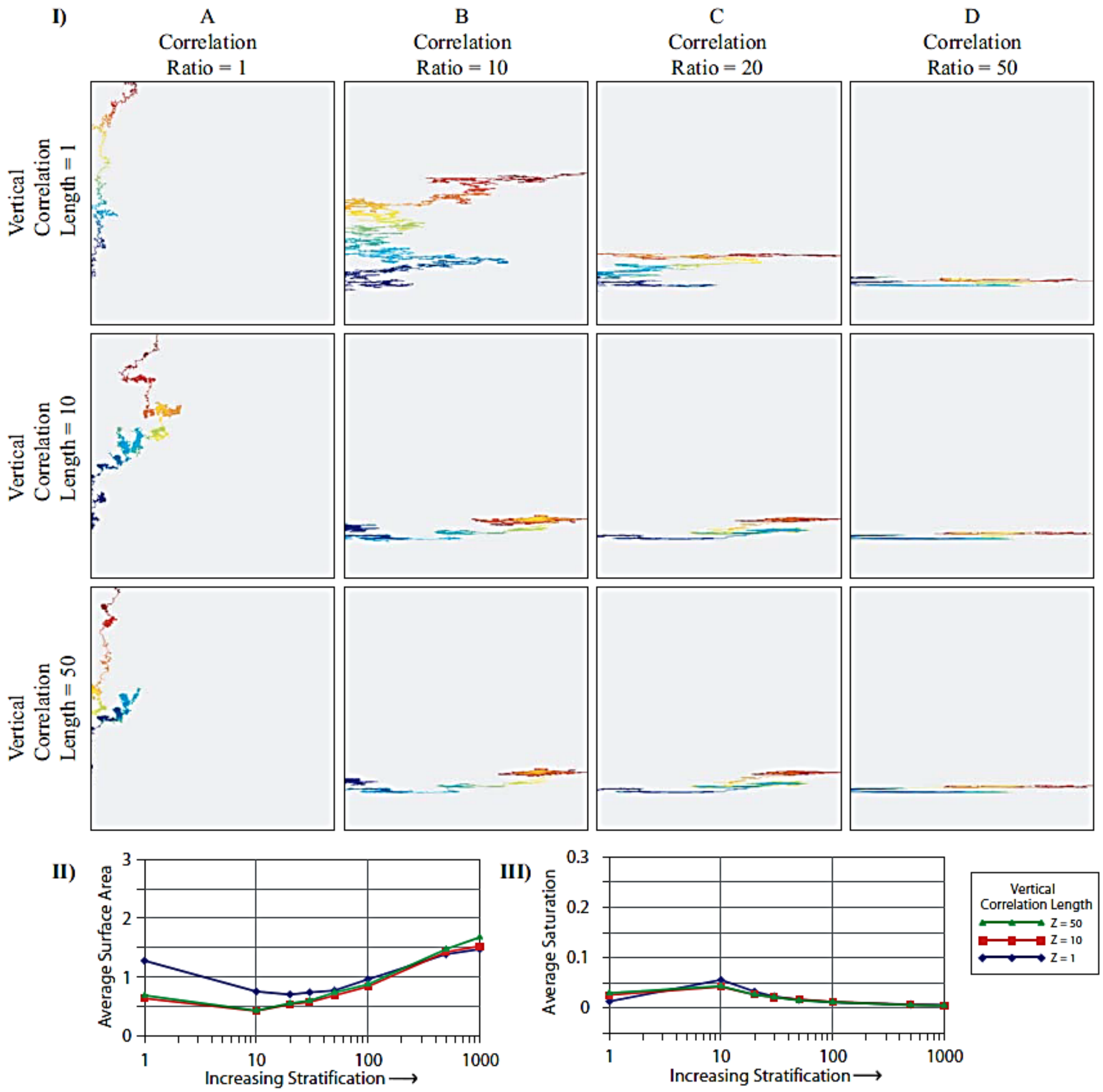

Figure 5. CO_2 invasion history (I) from a line source with a Bond Number = 0.1 and no viscous forces in (a) unstructured media, (b) weakly stratified media, (c) more stratified media, and (d) highly stratified media. Invasion pictures for correlation ratios of 100, 500, and 1000 are not shown because the invasion phase only populates a few layers near the bottom of the domain. CO_2 invasion progress from early to late is reflected by the progression of dark to light colors. Grid blocks saturated with the wetted phase are shown in gray. Plots displaying the (II) average surface area, and (III) average saturation for theses simulations versus increasing stratification. The average saturation is plotted between -0.5 to 0.3 to clearly illustrate results close to zero. No simulations produced saturations less than zero.

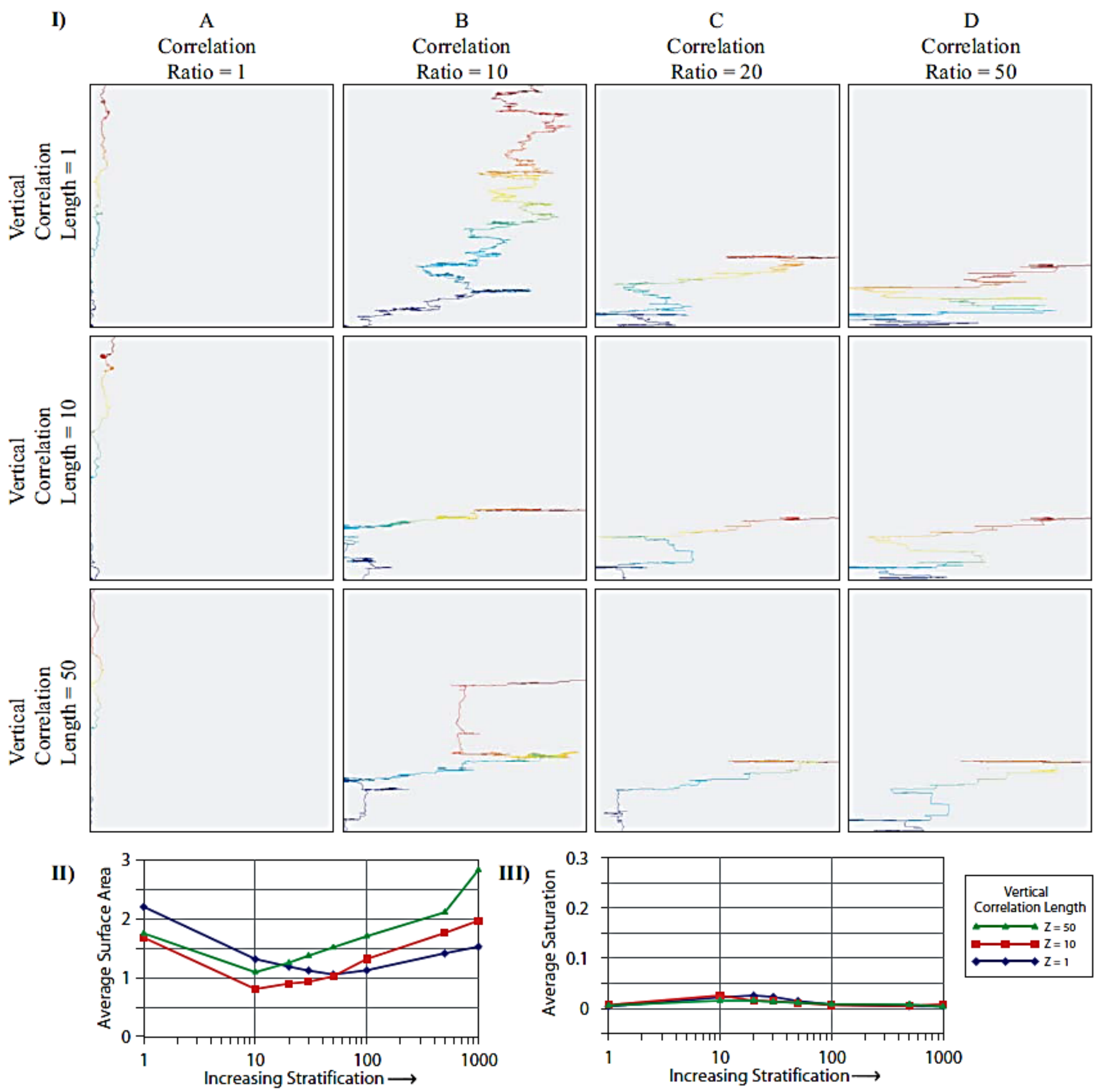

Figure 6. CO_2 invasion history (I) from a point source with a Bond Number = 1 and no viscous forces in (a) unstructured media, (b) weakly stratified media, (c) more stratified media, and (d) highly stratified media. Invasion pictures for correlation ratios of 100, 500, and 1000 are not shown because the invasion phase only populates a few layers near the bottom of the domain. CO_2 invasion progress from early to late is reflected by the progression of dark to light colors. Grid blocks saturated with the wetted phase are shown in gray. Plots displaying the (II) average surface area, and (III) average saturation for theses simulations versus increasing stratification. The average saturation is plotted between -0.5 to 0.3 to clearly illustrate results close to zero. No simulations produced saturations less than zero.

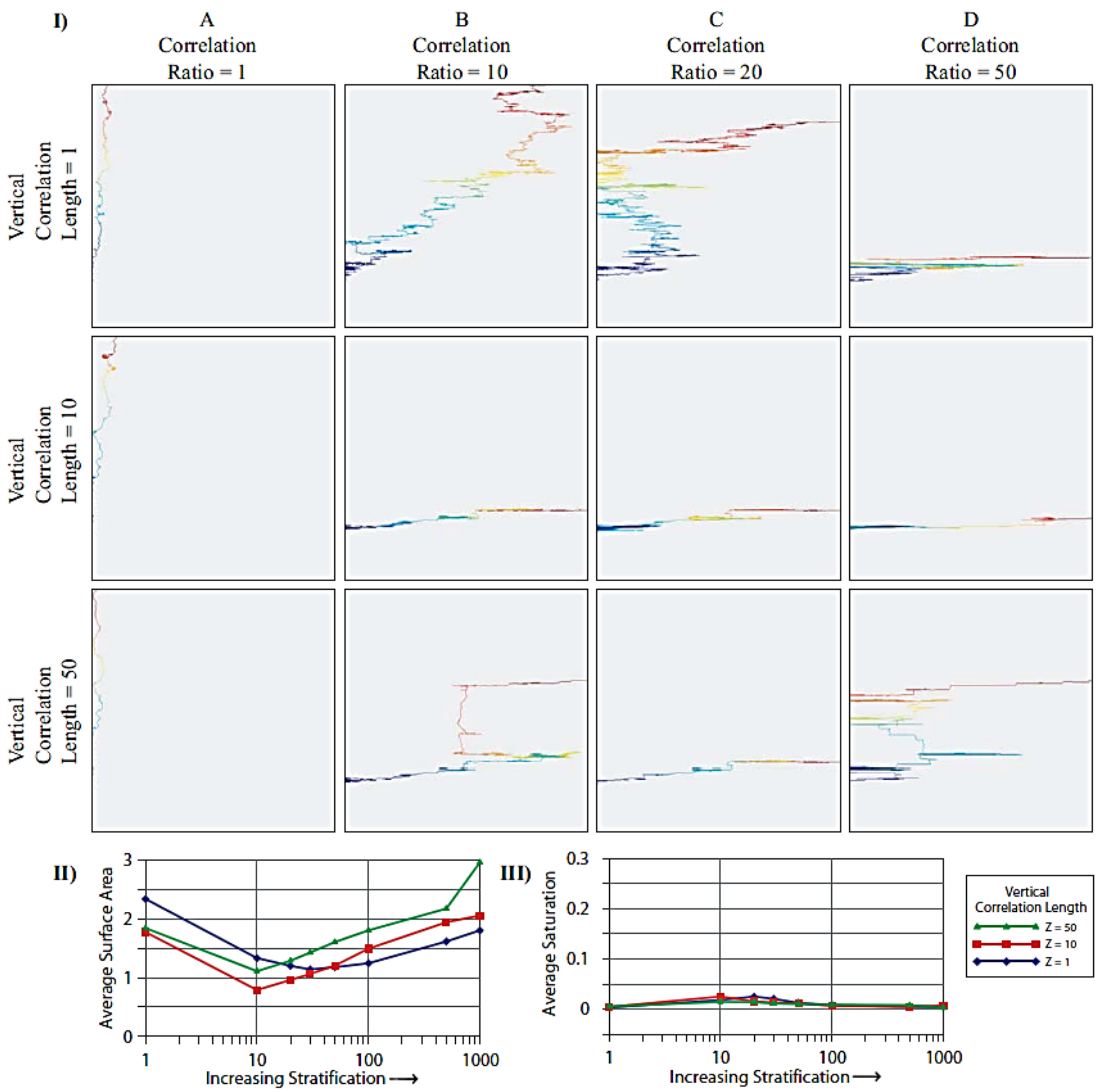

Figure 7. CO_2 invasion history (I) from a line source with a Bond Number = 1 and no viscous forces in (a) unstructured media, (b) weakly stratified media, (c) more stratified media, and (d) highly stratified media. Invasion pictures for correlation ratios of 100, 500, and 1000 are not shown because the invasion phase only populates a few layers near the bottom of the domain. CO_2 invasion progress from early to late is reflected by the progression of dark to light colors. Grid blocks saturated with the wetted phase are shown in gray. Plots displaying the (II) average surface area, and (III) average saturation for theses simulations versus increasing stratification. The average saturation is plotted between -0.5 to 0.3 to clearly illustrate results close to zero. No simulations produced saturations less than zero.

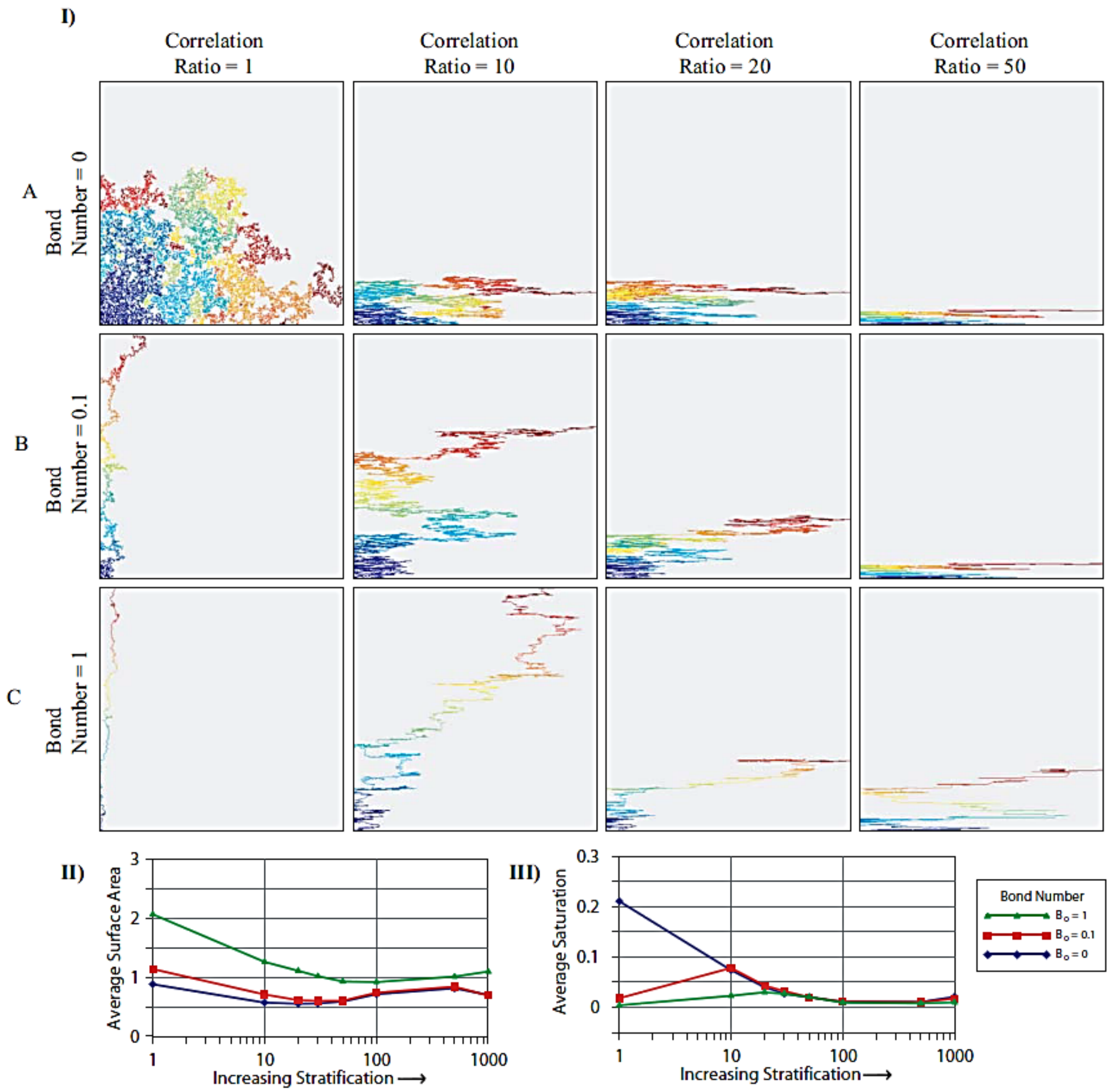

Figure 8. CO_2 invasion history (I) from a point source with VSN = 250 with Bon Numbers of (A) 0, (B) 0.1, (C) 1. Invasion pictures for correlation ratios of 100, 500, and 1000 are not shown because the invasion phase only populates a few layers near the bottom of the domain. CO_2 invasion progress from early to late is reflected by the progression of dark to light colors. Grid blocks saturated with the wetted phase are shown in gray. Plots displaying the (II) average surface area, and (III) average saturation for theses simulations versus increasing stratification. The average saturation is plotted between -0.5 to 0.3 to clearly illustrate results close to zero. No simulations produced saturations less than zero.

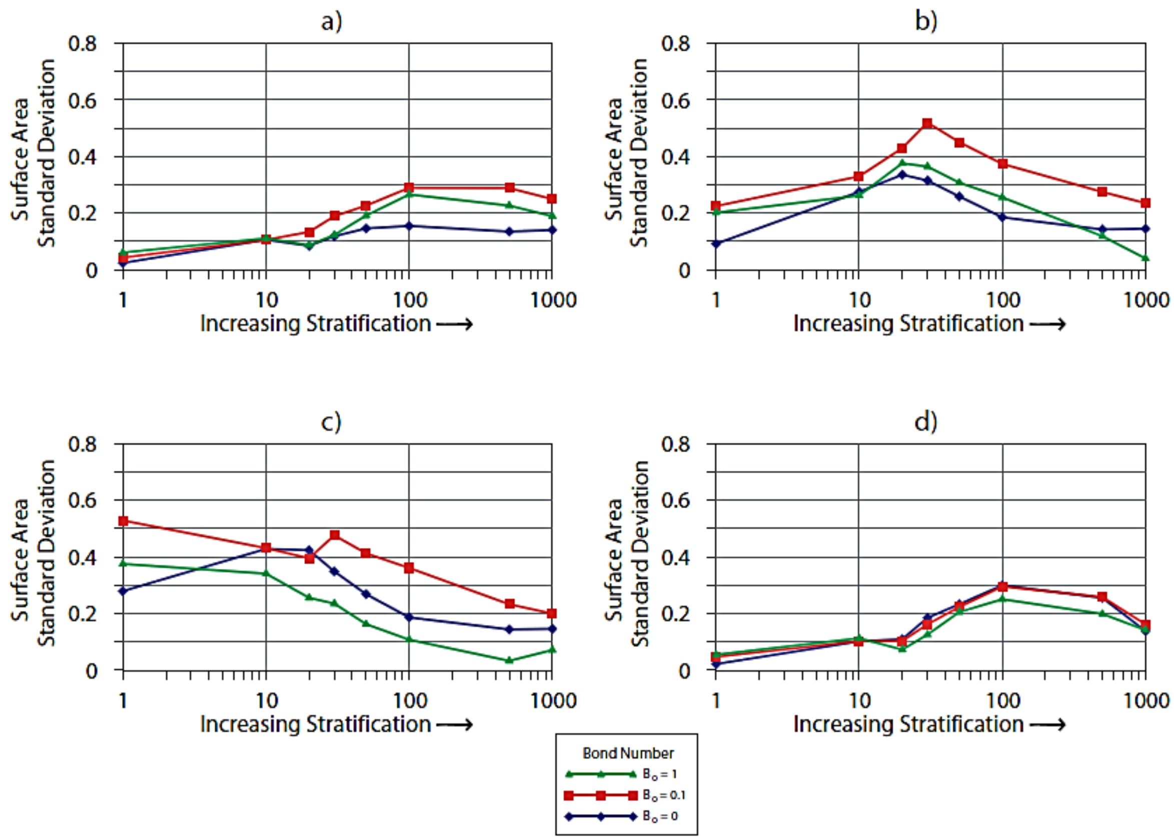

Figure 9. Plots displaying the coefficient of variation (*Cv*) of the CO_2 surface area for correlation lengths of (a) 1, (b) 10, and (c) 50 from a line source. Plot (d) displaying *Cv* of the CO_2 surface area for a correlation of 1 with a VSN = 250 invading from a point source.

Appendix: B

The appendix for this paper is not attached. It includes a copy of the program code, user manuals, and all program files.

VITA

Name: Frank G. Roecker

Address: Department of Geology and Geological Engineering
120 Carrier Hall
University, MS 38677

Education: B.S. Geological Engineering, The University of Mississippi, 2005